

Effect of Grain Structure Anisotropy and Recrystallization on Tensile Properties of Swaged Tungsten Rod

Wenhai GUAN, Shuhei NOGAMI, Makoto FUKUDA, Atsuo SAKATA and Akira HASEGAWA

Department of Quantum Science and Energy Engineering, Tohoku University, Sendai 980-8579, Japan

(Received 24 December 2014 / Accepted 6 July 2015)

Tungsten (W) is considered as primary candidates for plasma-facing materials (PFM) in current fusion reactor designs because of their high melting point and high sputtering resistance. In this study, pure W rods fabricated by a swaging process and having two different diameters (6 and 10 mm) are examined. To investigate the effect of anisotropy and recrystallization on the tensile properties of W rod, grain structure, hardness, tensile strength and elongation, and fracture surfaces are observed or measured for as-received and heat-treated materials. Based on grain structure observation and tensile tests, the axial and radial directions of W rod show different microstructures, called microstructure anisotropy due to swaging. A significant anisotropy of tensile properties is observed in as-received W rods at room temperature. Tensile strength of the rod with smaller diameter is higher than that of the one with larger diameter, and plastic deformation is observed only for the as-received smaller diameter rod, in further measurements at room temperature. However, when tested at 773 K there is no obvious anisotropy of tensile properties observed in as-received and heat-treated materials. Through these comparisons, the smaller diameter rod material shows better tensile properties than the one with larger diameter because of its higher reduction ratio. The reduction ratio plays an important role in affecting the microstructure and tensile properties of W rod material.

© 2015 The Japan Society of Plasma Science and Nuclear Fusion Research

Keywords: tungsten, anisotropy, recrystallization, grain structure, hardness, tensile property

DOI: 10.1585/pfr.10.1405073

1. Introduction

Tungsten (W) is considered as primary candidate for plasma-facing materials (PFM) of the divertor and blanket first wall in current fusion reactor designs because of its high melting point and high sputtering resistance. However, W has drawbacks such as a high ductile-to-brittle transition temperature (DBTT) [1], recrystallization embrittlement [2], and irradiation embrittlement and hardening [3–8].

The microstructure and tensile properties of W are strongly dependent on its fabrication method and history. Differing microstructure in different directions can result during fabrication of W plate and rod, and cause variation in the tensile properties in these directions, i.e., anisotropy. For example, in a W plate fabricated by rolling, an elongated and non-equiaxed grain structure has been observed along the rolling direction [9]. In addition, it is well-known that the tensile properties are affected by both grain growth and coarsening that are due to recrystallization at elevated temperature. Therefore, in order to use W for PFM, the characteristics of microstructure, tensile property, and recrystallization behavior should be taken into account.

Pure W rod is commonly fabricated by a swaging process. The W parent metal ingot is manufactured by powder metallurgy [10]; subsequently, a W rod with the tar-

get diameter is obtained by swaging [11]. During swaging, formation of different grain shapes in the axial and radial directions is expected, and anisotropy in microstructure and tensile properties can occur in pure W rod [12, 13]. Therefore, quantitative measurements of grain structure, strength, and elongation are needed in each direction of pure W rod. In addition, recrystallization will cause variation and anisotropy of tensile properties. For PFM applications, the effects of recrystallization on anisotropy of microstructure and tensile properties in swaged W rod should also be investigated. Furthermore, in the swaging process, the pressure applied by a die in the radial direction depends on the diameter of rod formed, and the reduction ratio in the radial direction may be important in determining grain size and grain structure. Therefore, the effects of reduction ratios on properties in both axial and radial directions should be taken into account.

These aspects of W wire and rod have been studied, with several reports in recent years. For example, Peck et al. showed that a fiber structure exists in swaged W wire [11]. Meieran et al. reported a twisted fiber structure in drawn W wire [14]. Furthermore, both observed highly elongated grain structures along the axial direction of W wire and rod. After that, Lee reported that a drawn W wire has sufficient ductility at room temperature [15]. Reiser et al. and Uytendhouwen et al. showed high tensile strength in the axial direction and significant tensile anisotropy for

author's e-mail: wenhai.guan@jupiter.qse.tohoku.ac.jp

W rods fabricated by rolling [9, 12]. Tanoue et al. reported a relationship between higher workability and good tensile properties in swaged W rod [10]. However, little effort has been spent on studies of recrystallization behavior in swaged W rod, and the microstructure and tensile properties should be investigated to determine whether anisotropy exists in recrystallized rod material. Further, the effect of swaging diameter and reduction ratio on recrystallized rod material should be included.

The objective of this study is to investigate the effects of reduction ratio, anisotropy of tensile properties, and recrystallization behavior in swaged pure W rods.

2. Experimental

2.1 Materials and heat treatment

The materials examined in this study were two diameters of pure W rods. The rod diameters were 6 mm (labeled as T- ϕ 6), and 10 mm (labeled as T- ϕ 10). The pure W rods were fabricated by powder metallurgy and swaging, and supplied by TOHO KINZOKU Co., LTD., Japan. T- ϕ 6 and T- ϕ 10 were swaged from the same W billets. The reduction ratios of T- ϕ 6 and T- ϕ 10 were 90% and 75%, respectively. The reduction ratio of T- ϕ 6 is thus higher than that of T- ϕ 10. To evaluate recrystallization behavior, the T- ϕ 6 specimens were heat-treated at 1573 K or 1773 K, and T- ϕ 10 was heat-treated only at 1773 K; the heat treatments were of 1 h duration in a vacuum below 10^{-4} Pa, using an infrared gold image furnace. The heat treatment was labeled as HT and showed in table and figure.

2.2 Grain structure observation

The grain structure observation was carried out using an optical microscope (KEYENCE Corp., VHX-200). The as-received and heat-treated specimens were mechanically polished using waterproof abrasive papers up to #3000. Electrolytic polishing was then performed using a 1 wt.% sodium hydroxide aqueous solution. Finally, etching was performed using a mixed aqueous solution containing 10 wt.% potassium ferricyanide and 10 wt.% sodium hydroxide.

2.3 Vickers hardness measurement

Vickers hardness measurement of the as-received and heat-treated specimens was carried out using a Vickers hardness tester (SHIMADZU Corp., Micro Hardness Tester HMV-1 TADW). The specimens were polished using waterproof abrasive papers up to #3000 before hardness measurement. The test temperature, indentation load, and dwell time were: room temperature, 1.96 N, and 15 s, respectively.

2.4 Tensile test

The shape and geometry of the tensile specimens (i.e., VS-T1, VS-T8, and SS-J2 types) are shown in Figs. 1 (a), (b), and (c), respectively. The gauge section dimen-

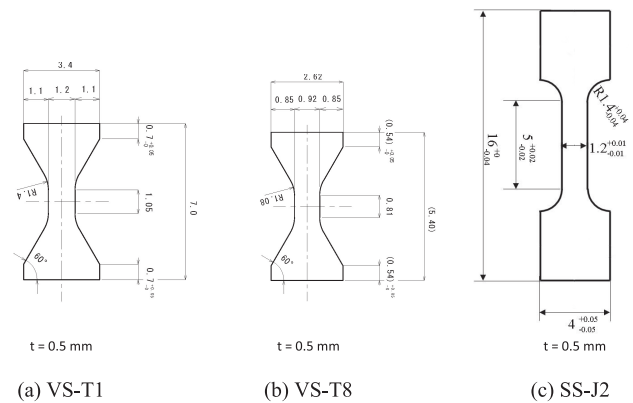


Fig. 1 Shape and geometry of the tensile specimens ((a) VS-T1, (b) VS-T8, and (c) SS-J2).

sions of the VS-T1, VS-T8, and SS-J2 specimens were $1.05 \text{ mm} \times 1.2 \text{ mm} \times 0.5 \text{ mm}$, $0.81 \text{ mm} \times 0.92 \text{ mm} \times 0.5 \text{ mm}$, and $5 \text{ mm} \times 1.2 \text{ mm} \times 0.5 \text{ mm}$, respectively. The loading axes of the tensile specimens, which were machined from the rod materials, were aligned with the axial (labeled as T- ϕ 6-Ax, T- ϕ 10-Ax) and radial directions (labeled as T- ϕ 6-Rad, T- ϕ 10-Rad) of the rods. The gauge section of the tensile specimens was taken from the radial center region of the rod materials. The test specimen surfaces were polished along the loading axis direction using #1500 waterproof abrasive papers.

Tensile tests were carried out at room temperature in air and at 773 K in a vacuum below 10^{-4} Pa, using an electromotive testing machine with 2 kN load cell (INTESCO Co., LTD., Japan). Based on the DBTT of pure W fabricated by swaging process in previous research, the DBTT was in the temperature range from room temperature to 773 K [16]. Thus, to investigate the tensile properties of brittle and ductile W rod, the temperature below and above DBTT were considered in this study. The axial strain was estimated from the testing machine cross-head displacement. The strain rate was 10^{-3} s^{-1} . After the tensile tests, fracture surfaces were examined using a scanning electron microscope (SEM) (JSM-5310LV, JEOL Ltd.).

3. Results and Discussion

3.1 Grain structure

Grain structures of the as-received and heat-treated W rods (T- ϕ 6 and T- ϕ 10) are shown in Fig. 2. The relationship among average grain size, aspect ratio, and reduction ratio of as-received T- ϕ 6 and T- ϕ 10 are listed in Table 1. The as-received rod materials exhibit distinct grain structures. The radial surface of as-received T- ϕ 6 and T- ϕ 10 rods show an equiaxed grain structure. T- ϕ 6 has a relatively smaller grain than T- ϕ 10. On the axial surface, the as-received T- ϕ 6 and T- ϕ 10 rods show elongated grain structure. However, the T- ϕ 6 rod has a slender, longer, and straighter grain structure regularly distributed along the rod

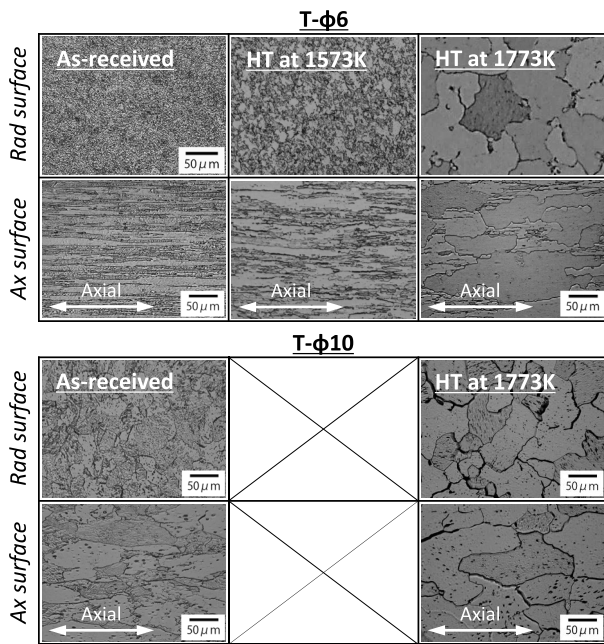


Fig. 2 Grain structures of the as-received and heat-treated W rods (T-φ6 and T-φ10).

Table 1 Average grain size, aspect ratio and reduction ratio of T-φ6 and T-φ10.

	T-φ6	T-φ10
Length, μm	87	53
Diameter, μm	15	24
Aspect ratio	5.8	2.2
Reduction ratio, %	90	75

axis than the T-φ10 rod. The grain structures of these W rods might be related to the different reduction ratios in the swaging process. Swaging has been observed to form an elongated grain structure along the rod axis and an aggregated structure described as fiber texture [12, 13].

After heat treatment at 1573 K, slight grain growth is observed in the radial and axial surfaces in the T-φ6 rod, and it might indicate that the recrystallization start temperature for the T-φ6 rod is 1573 K. After heat treatment at 1773 K, obvious grain growth in the radial and axial surfaces is observed in the T-φ6 and T-φ10 rods, due to recrystallization. The elongated grain structure in the axial direction has disappeared, and has changed into an equiaxed grain structure by grain growth and grain coarsening.

3.2 Vickers hardness

Figure 3 shows the relationship between heat treatment temperature and Vickers hardness of the W rods,

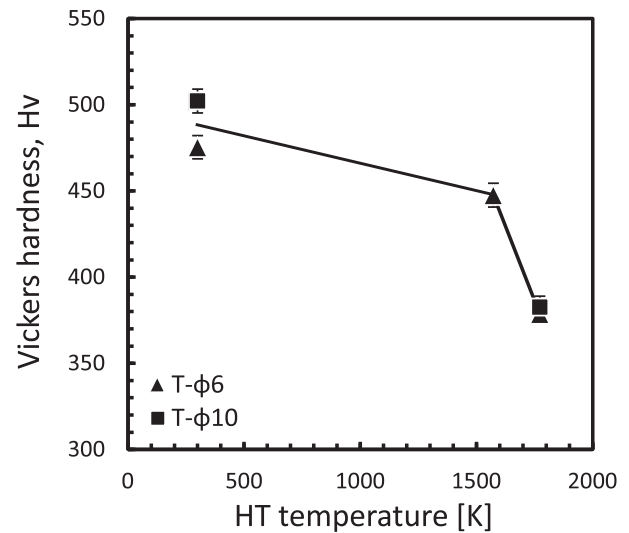


Fig. 3 Relationship between the heat treatment (HT) temperature and the Vickers hardness of the W rods (T-φ6 and T-φ10).

T-φ6 and T-φ10. For each treatment (as-received, heat-treated at 1573 K or 1773 K), specimens show the same hardness value on radial and axial surfaces, and we show only the radial surface results. The hardness over the radial surface of each specimen rod ranges within a few percent (5%) of the average values plotted in Fig. 3.

A slight reduction of hardness is observed in the specimen heat-treated at 1573 K and a significant reduction of hardness is observed in the specimen heat-treated at 1773 K. These might be caused by grain growth. Combining the results of hardness test with grain structure observation analysis, the recrystallization already starts at 1573 K.

3.3 Tensile properties

Table 2 shows a summary of the tensile tests of pure W rods. The test temperature, heat treatment temperature, orientation of the loading axis to the rod material direction (T-φ6-Ax, T-φ10-Ax, T-φ6-Rad, T-φ10-Rad), specimen type (VS-T1, VS-T8, and the SS-J2), ultimate tensile strength (UTS), 0.2% proof stress ($\sigma_{0.2}$), and the fracture manner are listed in Table 2. Because of the limitations of the rod material and specimen size, a standard specimen could not be fabricated for this study, and VS-T1, VS-T8, and SS-J2 type specimens were used for the tensile tests. SS-J2 type of tensile specimens were used for investigating the tensile properties of rod axis. VS-T1 and VS-T8 types of tensile specimens were used for evaluating the anisotropy of T-φ6 and T-φ10, respectively. The VS-T1, VS-T8, and SS-J2 type specimens showed almost the same strength compared to standard specimens in our previous test and work. However, because their size and shoulder design of specimen (Figs. 1 (a) and (b)) resulted in easier sliding between the jig and specimen than standard specimen, the specimen types used in this study showed different elongations

Table 2 Summary of the tensile tests.

Test temp. [K]	HT temp. [K]	Material	Specimen	UTS [MPa]	$\sigma_{0.2}^*$ [MPa]	Fracture manner		
						Fracture surface	Necking and slip band	Cracks in specimen surface
RT***	AR**	T-φ6-Ax	VS-T1 SS-J2	1218–1457	1260–1420	Cleavage	no	no
		T-φ10-Ax	VS-T1	661	—	Cleavage	no	no
		T-φ6-Rad	VS-T8	524	—	Cleavage	no	no
		T-φ10-Rad	VS-T1	255	—	Cleavage	no	no
	1573	T-φ6-Ax	SS-J2	1342–1389	—	Cleavage	no	no
		T-φ10-Ax				<i>Not-tested</i>		
		T-φ6-Rad				<i>Not-tested</i>		
		T-φ10-Rad				<i>Not-tested</i>		
	1773	T-φ6-Ax	SS-J2	560–827	—	Partly intergranular	no	no
		T-φ10-Ax				<i>Not-tested</i>		
		T-φ6-Rad				<i>Not-tested</i>		
		T-φ10-Rad				<i>Not-tested</i>		
773	AR**	T-φ6-Ax	VS-T1	579	530	Ductile	yes	no
		T-φ10-Ax	VS-T1	540	526	Ductile	yes	no
		T-φ6-Rad	VS-T8	506	460	Ductile	yes	yes
		T-φ10-Rad	VS-T1	517	496	Cleavage	yes	yes
	1773	T-φ6-Ax	VS-T1	378	240	Ductile	yes	no
		T-φ10-Ax	VS-T1	330	126	Ductile	yes	no
		T-φ6-Rad	VS-T8	427	328	Ductile	yes	no
		T-φ10-Rad	VS-T1	334	112	Ductile	yes	no

*The $\sigma_{0.2}$ of materials that showed no yielding is labeled as “—”.

**AR: As-received

***RT: Room temperature

during tensile tests.

3.3.1 Effect of recrystallization

Figure 4 shows results of the tensile test at room temperature for the rod axial direction of as-received and heat-treated specimens (T-φ6-Ax). Shown are the stress-strain curves and SEM images of the fracture surfaces. The specimen heat-treated at 1573 K shows slightly lower strength than the as-received specimen, because the recrystallization already starts at 1573 K. Further, the specimen heat-treated at 1773 K shows the lowest strength due to recrystallization [13]; on the other hand, it does not show plastic deformation and yield point. All specimens show a cleavage fracture pattern; however, the as-received and 1573 K

heat-treated specimens exhibit a transgranular fracture and river pattern. On the other hand, the fracture surface of the 1773 K heat-treated specimen exhibits a partly intergranular fracture. In addition, the as-received and 1573 K heat-treated specimens have a yield point and more elongation than the 1773 K specimen, as shown in Fig. 4. In other words, based on the results of the tensile test for T-φ6-Ax at room temperature, the un-recrystallized specimen has a great degree of ductility and a capacity to deform. The continual and regular fiber structures along axial direction were observed in as-received T-φ6 (Fig. 2). On the other hand, T-φ10 showed the disorderly and discrete grain structures along the axial direction. Furthermore, fiber structures of T-φ6-Ax appear to be twisted along its axial direction as well as being bent, forming a bent and

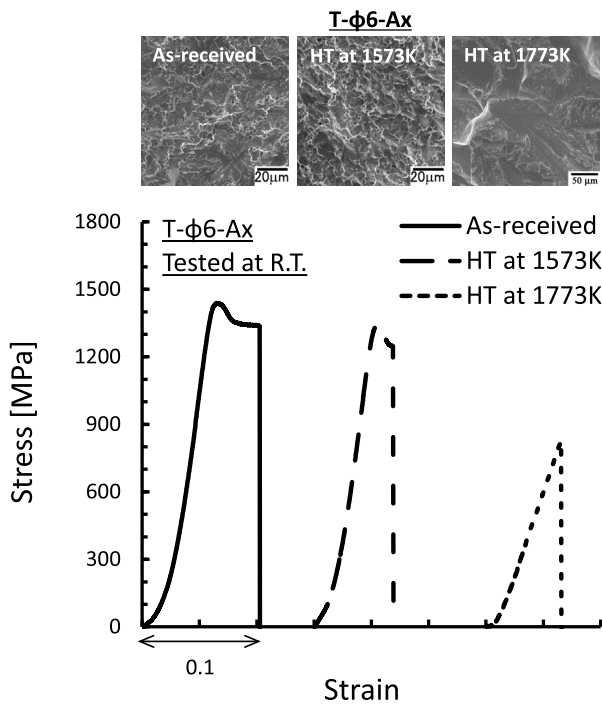


Fig. 4 Stress-strain curves of the tensile test at room temperature and fracture surfaces after the test of the as-received and heat-treated W rod (T-φ6-Ax).

twisted structure called interlock boundary that was caused by swaging process rotary of dies [11]. However, these fiber structures were not observed in T-φ10-Ax. These fiber structures were important because they bring better ductility along axial direction of T-φ6. Furthermore, the most of fiber state in swaged T-φ6 rod was fabricated by strong interlocked boundary that can keep a great ductility in deformation of uniaxial tensile test along axial direction. Overall, based on the fracture surfaces, all specimens show brittle fracture at room temperature. However, in comparison to the un-recrystallized specimens (as-received and 1573 K heat-treated), the fully recrystallized specimen exhibits around half the strength and no obvious plastic deformation at room temperature. The pure W rod shows completely different tensile properties before and after recrystallization. The as-received specimen at room temperature shows great strength and ductility, and these properties are similar to those noted in previous research [15].

Figure 5 shows the stress-strain curves of the as-received and heat-treated W rods (T-φ6-Ax, T-φ10-Ax, T-φ6-Rad, and T-φ10-Rad), tested at 773 K. For the axial-direction specimens (upper graph), as-received T-φ6 and T-φ10 show almost the same strength; heat-treated T-φ6 and T-φ10 also show almost the same strength as each other, but lower than the as-received specimens. The elongation of as-received T-φ6 is approximately 20% and 40% larger than as-received T-φ10 along axial direction and radial direction, respectively; however, there is no significant difference in elongation between heat-treated T-φ6 and T-

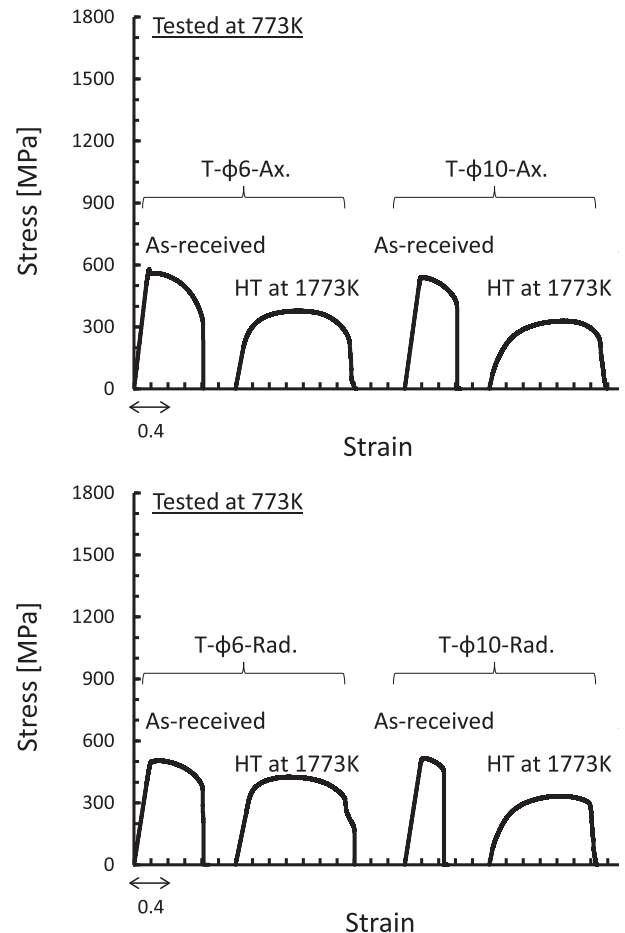


Fig. 5 Stress-strain curves of the tensile test at 773 K of the as-received and heat-treated W rods (T-φ6-Ax, T-φ6-Rad, T-φ10-Ax, and T-φ10-Rad).

φ10. In comparison, for the radial-direction specimens (lower graph), a similar pattern is seen as with the axial-direction specimens. As-received T-φ6 and T-φ10 again show almost the same strength; heat-treated T-φ6 and T-φ10 also show almost the same strength as each other, but lower than the as-received specimens. The elongation is the same as for the axial direction specimens, with differences between as-received and heat-treated specimens, and between T-φ6 and T-φ10 for as-received specimens. Although the strength of recrystallized specimens was lower than that of as-received specimens at room temperature, the recrystallized specimen showed favorable elongation at 773 K.

Results of the tensile test of T-φ6 and T-φ10 were evaluated along with details of the fracture manner as shown in Fig. 6; the fracture surface, top surface, and side surface are shown. The fracture manner for as-received T-φ6-Ax tested at room temperature, shown in Fig. 6(a), is cleavage. A river pattern is observed on the fracture surface. Other examples of as-received specimens fracture surface in room temperature tests are similar to T-φ6-Ax because of the brittleness characteristic of W at room tem-

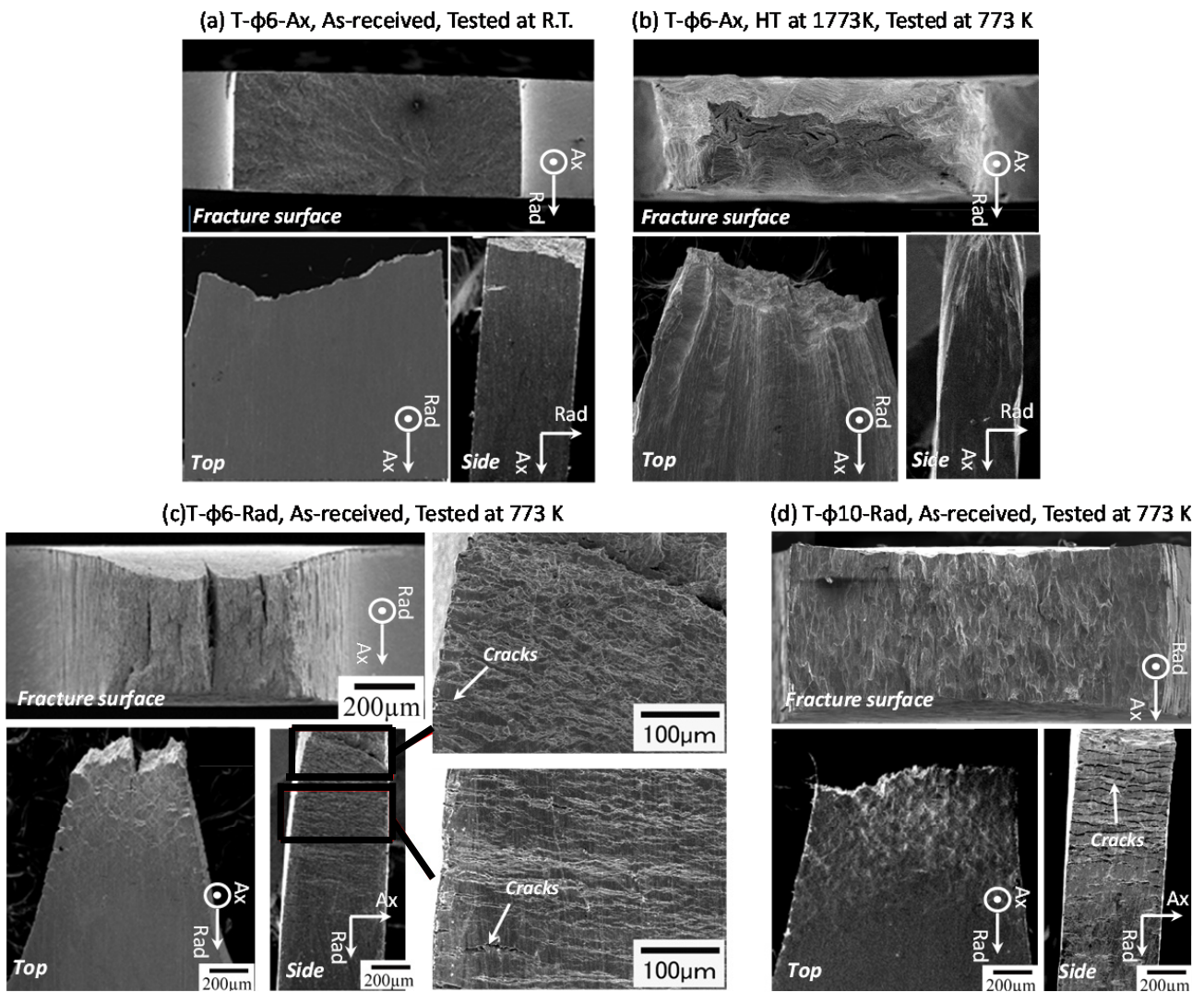


Fig. 6 Typical fracture surface, top surface, and side surface of fracture.

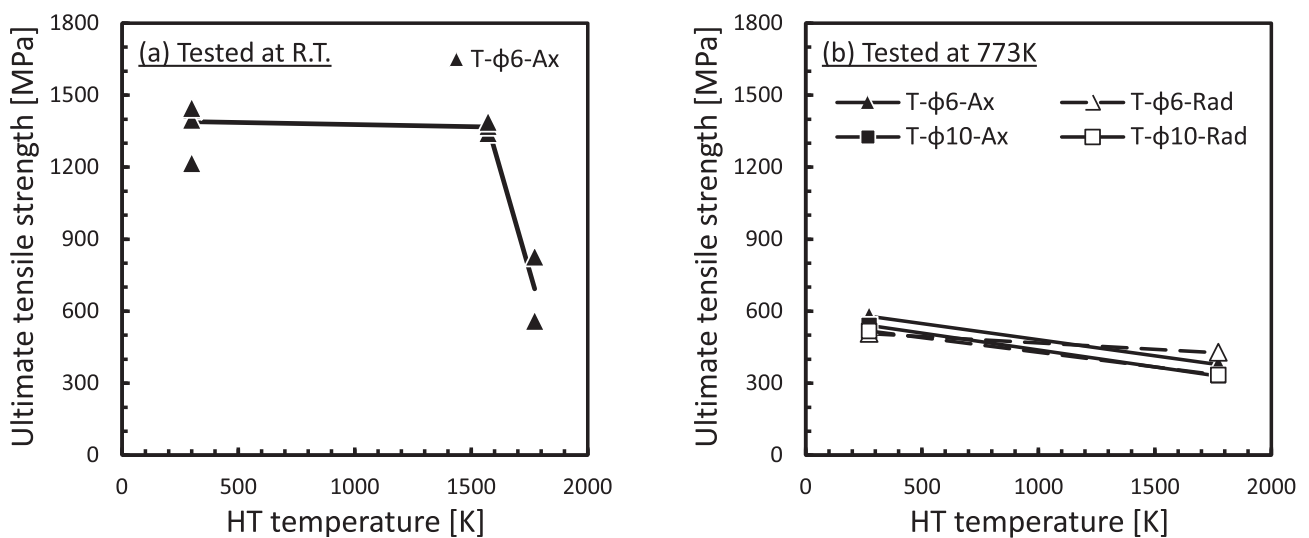


Fig. 7 Relationship between the heat treatment (HT) temperature and the UTS at (a) room temperature and (b) at 773 K of the W rods (T-φ6-Ax, T-φ6-Rad, T-φ10-Ax, and T-φ10-Rad).

perature. In the case of heat-treated T- ϕ 6-Ax tested at 773 K, Fig. 6(b), the fracture manner is ductile. A dimple is observed on the fracture surface. The other cases of heat-treated specimens at 773 K are similar to heat-treated T- ϕ 6-Ax. In the case of as-received T- ϕ 6-Rad at 773 K, the fracture manner is ductile, and the fracture surface consists of some cracks along the axial direction (rod axis) of tensile specimens as indicated in Fig. 6(c). A slip line and plastic deformation are observed on the top surface. In addition, the side surface showed some small cracks along the axial direction (rod axis) of the tensile specimen. In the case of as-received T- ϕ 10-Rad at 773 K, the fracture manner is cleavage. A slip line and plastic deformation are observed on the top surface. In addition, the side surface contains cracks along the axial direction (rod axis) of the tensile specimen. In these two cases, the cracks might be formed by the separation of fibers along grain boundaries. As indicated before, the grain structure in the axial direction is aggregated and forms fiber structures that dominate the characteristic of W rod. The process of fracture was influenced more by properties of the fibers (i.e., the fiber length and imperfections in the fibers) than by the specific nature of the fiber interface [15]. Therefore, the reason might be that circumferential stress is induced by tensile stress during testing. When circumferential stress reaches sufficient magnitude in the necked region, cracks might occur at fiber interfaces along the weak-linked grain boundaries. Furthermore, when the reduction ratio is increased, cracks have difficulty propagating, and grain boundary sliding easily occurs in material at elevated temperature. The T- ϕ 6 specimen has a more strongly coupled grain structure than T- ϕ 10. As a result, T- ϕ 10 shows obvious cracks on the side surface of the specimen. A weak-linked grain boundary may have existed in the radial direction of the rod material.

The effect of recrystallization on tensile properties of W rods is examined in this study; the relationship between heat treatment temperature and UTS at room temperature and 773 K is summarized in Fig. 7. In room temperature tests (Fig. 7(a)), the specimen heat-treated at 1573 K shows slightly lower UTS than the as-received specimen. This means that for heat treatment at or below 1573 K, there might not be a significant change of tensile properties in pure W rod. However, the UTS of some heat-treated specimens is obviously lower than others. As indicated before, recrystallization causes decreased tensile strength at room temperature. According to the Hall-Patch relation, materials with smaller grain sizes exhibit greater strength than ones with larger grains [17], thus, the UTS at room temperature of as-received specimens is higher than that of recrystallized specimens. On the other hand, as supported by the heat-treatment dependence of UTS at 773 K (Fig. 7(b)), the strength of W rod material in the high temperature region is not expected to be strongly dependent on grain size and shape because the material is far more likely to contain dislocation glides. Both the as-received speci-

men and the recrystallized specimen show lower strength at 773 K than at room temperature. Nonetheless, the UTS of recrystallized specimens is lower than that of as-received specimens at 773 K.

Incorporating grain structure and tensile test results, the fiber structure and interlock boundary were observed in axial direction of as-received T- ϕ 6 that showed greater tensile strength and elongation than T- ϕ 10 at room temperature due to the high reduction ratio. However, these phenomena were not observed in as-received T- ϕ 10 because of the relative low reduction ratio, disorder and discontinuity grain structure along rod axis. After heat treatment at 1773 K, instead of the fiber structure, equiaxed grain structure were observed in T- ϕ 6 and T- ϕ 10 due to the fully recrystallization. From the stress-strain curves at 773 K and summary, the elongation for the heat-treated specimen is more than two times larger than for the as-received specimen. The fully recrystallized specimens show almost the same strength and elongation, regardless of the rod diameter.

In this high temperature region, the strength in the radial direction of the rod does not change as much as in the axial direction. The anisotropy disappeared in as-received material due to the dislocation movement during high testing temperature region. In addition, from the perspective of tensile properties, the as-received T- ϕ 6 rod specimen showed greater tensile strength and elongation than T- ϕ 10 at room temperature and at 773 K. No obvious anisotropy was observed from the as-received and heat-treated specimens at 773 K.

3.3.2 Effect of grain anisotropy

Figure 8 shows the stress-strain curves at room temperature of as-received W rods; T- ϕ 6-Ax, T- ϕ 10-Ax, T- ϕ 6-

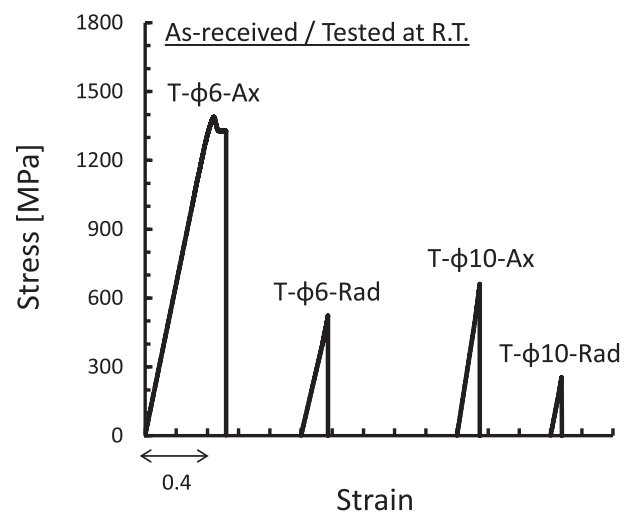


Fig. 8 Stress-strain curves of the tensile test at room temperature of the as-received W rods (T- ϕ 6-Ax, T- ϕ 6-Rad, T- ϕ 10-Ax, and T- ϕ 10-Rad).

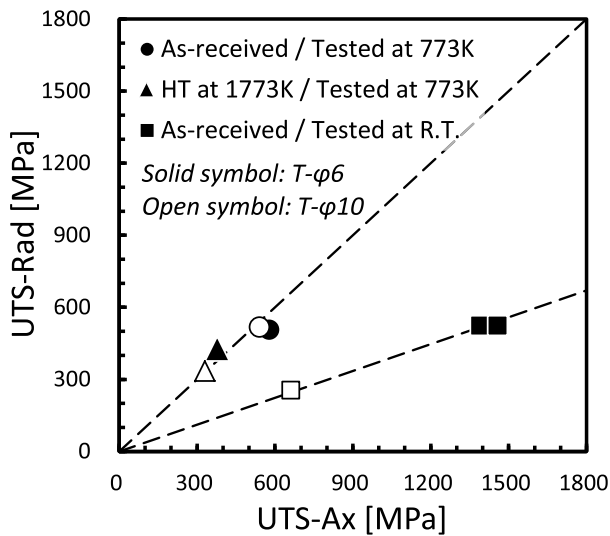


Fig. 9 Relationship between the UTS-Ax and UTS-Rad of the W rods (T- ϕ 6 and T- ϕ 10). (UTS-Ax: UTS of the test along the axial direction, UTS-Rad: UTS of the test along the radial direction).

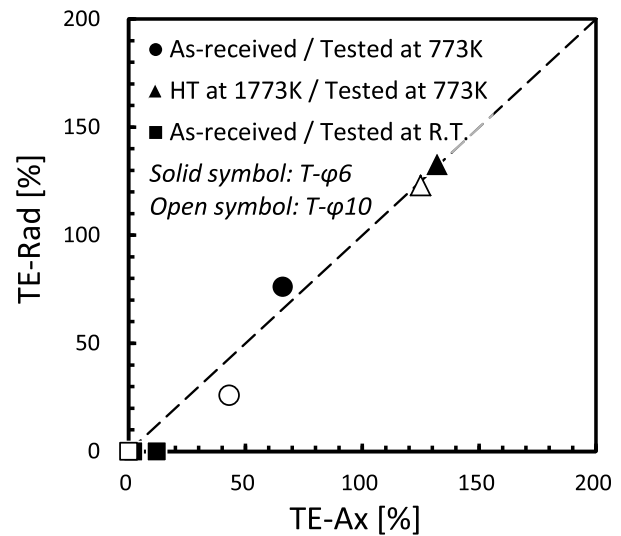


Fig. 10 Relationship between the TE-Ax and TE-Rad of the W rods (T- ϕ 6 and T- ϕ 10). (TE-Ax: TE of the test along the axial direction, TE-Rad: TE of the test along the radial direction).

Rad, and T- ϕ 10-Rad designate the rod diameter and test direction. As mentioned above, to investigate the characteristic of rod anisotropy, the VS-T1 (T- ϕ 10) and VS-T8 (T- ϕ 6) type of tensile specimen were introduced into this study because the diameter of W rod (no matter of T- ϕ 6 and T- ϕ 10) was not fit for the length of SS-J2 (geometry was shown in Fig. 1). From the stress-strain curves in Figs. 5 and 8, the UTS and total elongation (TE) were estimated for evaluating the effect of grain anisotropy. These also include tests at 773 K and heat-treated samples.

- 1) UTS-Ax: UTS of the test along the axial direction of the pure W rods.
- 2) UTS-Rad: UTS of the test along the radial direction of the pure W rods.
- 3) TE-Ax: TE of the test along the axial direction of the pure W rods.
- 4) TE-Rad: TE of the test along the radial direction of the pure W rods.

The relationships between UTS-Ax and UTS-Rad, and between TE-Ax and TE-Rad are shown in Figs. 9 and 10, respectively. The values of UTS and TE in the radial and axial directions are distributed around the diagonal of the figure. The UTS values of as-received T- ϕ 6 and T- ϕ 10 are distributed on the lower right section of Fig. 9, indicating that there is significant anisotropy at room temperature. Meanwhile, the UTS and TE of as-received and heat-treated T- ϕ 6 and T- ϕ 10 at 773 K are distributed around the diagonal of Figs. 9 and 10, which means there is no obvious anisotropy in the as-received and heat-treated specimens at 773 K.

Based on the grain structure observations and tensile tests, T- ϕ 6 shows a highly elongated grain structure along the rod axis, and great strength and elongation. As indi-

cated before, these elongated grain structures form fiber structures along the axial direction of pure W rod. As well, these fiber textures show little bending. These results for T- ϕ 6 on grain structure, strength and elongation are in agreement with previous reports [15, 18]. In comparison to material having a random crystal orientation, previous research has reported that fiber structures can improve the resistance to plastic deformation [19].

Unlike the T- ϕ 6 rod, as mentioned earlier, T- ϕ 10 shows shorter and stouter grain structure in the axial direction. Although the T- ϕ 10 rod was fabricated by the same process as T- ϕ 6, the differing microstructure and tensile properties demonstrate the effects of differing reduction ratios between T- ϕ 6 and T- ϕ 10. Based on the grain structure observation, a higher reduction ratio creates a more highly elongated grain structure along the rod axis during swaging. Furthermore, from the tensile tests, the highly elongated grain structure shows good tensile properties in the axial direction.

In summary, the rod material exhibits anisotropy in its microstructure and tensile properties at room temperature. Further, swaging to different diameters results in different strength and elongation behavior, with the reduction ratio being an important parameter affecting the microstructure and tensile properties.

3.4 Application of swaged W rod in divertor

In the current design of International Thermonuclear Experimental Reactor (ITER), the divertor has to withstand very high heat fluxes in the order of 10-20 MW/m² and has to remove reaction ash, residual fuel, and eroded particles to keep the plasma at a high quality level [20]. The ITER divertor is made of W plate fabricated by rolling pro-

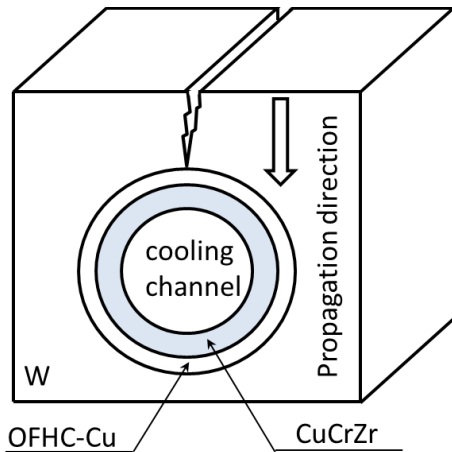


Fig. 11 The initial appearing position and propagation direction of ITER divertor.

cess. The crack was observed from plasma-facing surface to the vicinity of cooling channel under the heat load of 20 MW/m^2 totally 300 cycles [21, 22]. The initial appearing position and propagation direction of the crack were shown in Fig. 11 [23]. During heating period, the relatively lower temperature around 773 K of pure W which is expected to bring the possibility of the ductility, appears near the region of cooling channel of ITER divertor [23]. Furthermore, because the cracks were prone to be occurred during cooling period, the possibility of the ductility of W is desirable even at room temperature. No matter of direction of the pure W plate, the brittle fracture was observed below 473 K , and the ductility was not reported at direction of plate thickness below 1573 K [24]. On the other hand, this research of T- $\varphi 6$ has shown ductility along the axial direction at room temperature. However, T- $\varphi 10$ did not show any ductility with same situation. Thus, it is considered that the ductility is caused by the optimization of fabrication condition for reduction ratio and so on. Based on the initial appearing position and propagation direction of the crack in current design of ITER divertor, the tension and compression stress state along the Y-direction of divertor was occurred due to the cyclic heat loads. Therefore, the stress state along Y-direction in divertor should be paid more attention on. Because T- $\varphi 6$ has shown good ductility and strength along the axial direction in this study, the axial direction of W rod should be along the Y-direction of divertor during manufacture (Fig. 12). However, because of the relatively smaller diameter, the T- $\varphi 6$ was not fit for the current design of divertor. The adopting diameter of W rod was mainly decided by the size of parent material and reduction ratio. Therefore, manufacture of divertor with large diameter by W rod could be accomplished and ductility could be shown at room temperature based on certain optimization.

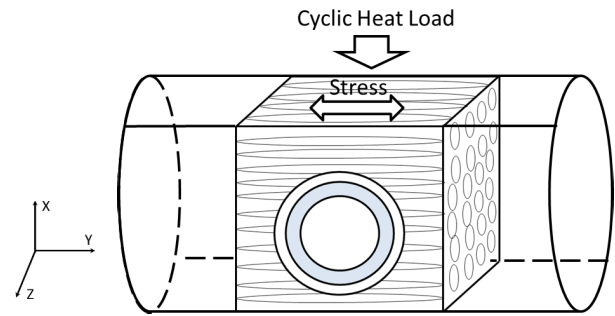


Fig. 12 Idea of W rod placed at appropriate direction for divertor manufacture.

4. Conclusions

To investigate the importance of anisotropies in microstructure and tensile properties, recrystallization behavior, and differing reduction ratios of swaged pure W rod, this study performed grain structure observation, hardness measurement, tensile tests, and fracture surface observation. The results are summarized as follows:

- 1) The as-received T- $\varphi 6$ and T- $\varphi 10$ exhibited grain structure anisotropy that the axial direction showed elongated grain structure and the radial direction showed equiaxed grain structure. A slight reduction of hardness and grain growth were observed after the heat treatment at 1573 K . Furthermore, the obvious grain growth and reduce strength were observed after the heat treatment at 1773 K . Therefore, the recrystallization of W rod already starts at 1573 K .
- 2) The grain structure anisotropy enables clear observations of significant increase of strength at axial direction and enhancement of the elongation in axial direction of the as-received T- $\varphi 6$ at room temperature. However, there was no obvious grain structure anisotropy of as-received T- $\varphi 6$ observed at 773 K . Due to the recrystallization, the strength was decreased and the elongation was increased in heat-treated T- $\varphi 6$. At the same time, the anisotropy disappeared. It might be caused by the dislocation movement during high testing temperature region.
- 3) At room temperature, T- $\varphi 6$ showed greater anisotropy than T- $\varphi 10$ both in grain structure and tensile properties. On the other hand, no matter of axial and radial direction of T- $\varphi 6$ and T- $\varphi 10$ at 773 K , the strength of these two was almost same, and elongation of as-received T- $\varphi 6$ was approximately 20% and 40% larger than as-received T- $\varphi 10$ along axial direction and radial direction, respectively. In addition, their strength and elongation are quite similar with each other after recrystallization. No obvious anisotropy was observed. The higher reduction ratio clearly leads to a finer grained and more pronounced anisotropic microstructure, at the same time, the fiber structure and interlock boundary can supply better ductility.

Therefore, the existence of ductility at room temperature strongly depends on strength of reduction ratio in swaged W rod. However, after recrystallization this effect is almost annihilated.

- 4) In this study, the higher swaging reduction ratio of W rod has shown better ductility and strength than lower one. The larger diameter of W rod fit for the present design of ITER divertor with a higher swaging reduction ratio should be discussed.

Acknowledgments

The authors are grateful to Dr. H. Kurishita and Dr. S. Matsuo for their help with tensile tests. This study was partly supported by a Grant-in-Aid for Scientific Research (B) 26289351 from the Ministry of Education, Culture, Sports, Science and Technology of Japan.

- [1] Q.Z. Yan, X.X. Zhang, T.N. Wang, C.T. Yang and C.C. Ge, *J. Nucl. Mater.* **442**, S233 (2013).
- [2] M. Fukuda, S. Nogami, A. Hasegawa, H. Usami, K. Yabuuchi and T. Muroga, *Fusion Eng. Des.* **89**, 1033 (2014).
- [3] M. Fukuda, A. Hasegawa, S. Nogami and K. Yabuuchi, *J. Nucl. Mater.* **449**, 213 (2014).
- [4] M. Fukuda, K. Yabuuchi, S. Nogami, A. Hasegawa and T. Tanaka, *J. Nucl. Mater.* **455**, 460 (2014).
- [5] T. Tanno, A. Hasegawa, J.C. He, M. Fujiwara, M. Satou, S. Nogami, K. Abe and T. Shishido, *J. Nucl. Mater.* **386-388**, 218 (2009).
- [6] A. Hasegawa, M. Fukuda, S. Nogami and K. Yabuuchi, *Fusion Eng. Des.* **89**, 1568 (2014).
- [7] V.S. Voitsenya, M. Balden, A.F. Bardamid, A.I. Belyaeva, V.N. Bondarenko, O.O. Skoryk, A.F. Shtan, S.I. Solodovchenko, V.A. Sterligov and B. Tyburska-Püschel, *J. Nucl. Mater.* **453**, 60 (2014).
- [8] S. Wurster, N. Baluc, M. Battabyal, T. Crosby, J. Du, C. García-Rosales, A. Hasegawa, A. Hoffmann, A. Kimura, H. Kurishita, R.J. Kurtz, H. Li, S. Noh, J. Reiser, J. Riesch, M. Rieth, W. Setyawan, M. Walter, J.H. You and R. Pippan, *J. Nucl. Mater.* **442**, S181 (2013).
- [9] J. Reiser, M. Rieth, B. Dafferner, S. Baumgärtner, R. Ziegler and A. Hoffmann, *Fusion Eng. Des.* **86**, 2949 (2011).
- [10] K. Tanoue, O. Nakano, H. Mori and H. Matsuda, *J. Japan Inst. Metals* **48**, 618 (1984).
- [11] J.F. Peck and D.A. Thomas, *Trans. Met. Soc. AIME* **221**, 1240 (1961).
- [12] I. Uytendhouwen, R. Chaouadi, J. Linke, V. Massaut and G.V. Oost, *Adv. Mater. Res.* **59**, 319 (2009).
- [13] W.F. Hosford, *Trans. Met. Soc. AIME* **230**, 12 (1964).
- [14] E.S. Meieran and D.A. Thomas, *Trans. Met. Soc. AIME* **233**, 937 (1965).
- [15] D. Lee, *Met. Trans.* **6A**, 2083 (1975).
- [16] R.J. Siegle and C.H. Li, *The Notch Impact Behavior of Tungsten*, Defense Documentation Center, Virginia (1963).
- [17] N.J. Petch, *J. Iron Steel Inst.* **173**, 25 (1953).
- [18] S. Leber, *Trans. Met. Soc. AIME* **233**, 953 (1965).
- [19] W.F. Hosford, *Texture Hardening* (Springer-Verlag, New York, 1969) pp. 414-435.
- [20] S. Suzuki, M. Akiba and M. Saito, *J. Plasma Fusion Res.* **82**, 699 (2006).
- [21] B. Riccardi, P. Gavila, R. Giniatulin, V. Kuznetsov, R. Rulev, N. Klimov, D. Kovalenko, V. Barsuk, V. Koidan and S. Korshunov, *Fusion Eng. Des.* **88**, 1673 (2013).
- [22] G. Pintsuk, I. Bobin-Vastra, S. Constans, P. Gavila, M. Rödiger and B. Riccardi, *Fusion Eng. Des.* **88**, 1858 (2013).
- [23] M. Fukuda, S. Nogami, A. Hasegawa, K. Yabuuchi, K. Ezato, S. Suzuki, H. Tamura and T. Muroga, *J. Plasma Fusion Res. SERIES* **11**, 099 (2015).
- [24] M. Fukuda, S. Nogami, K. Yabuuchi, A. Hasegawa and T. Muroga, presented at TOFE-2014, California, USA and to be published in *Fusion Sci. Technol.*